Irrigation & Drainage Systems Engineering

Research Article   **Open Access**

Computational Fluid Dynamics (CFD) Picture of Water Droplet Evaporation in Air

Giulio Lorenzini[1], Alessandra Conti[2] and Daniele De Wrachien[3]*

[1]*University of Parma, Department of Industrial Engineering, viale G.P. Usberti no.181/A, Parma 43124, Italy*
[2]*Alma Mater Studiorum-University of Bologna, Department of Energetic Nuclear and Environmental Control Engineering, viale Risorgimento no. 2, Bologna 40136, Italy*
[3]*Department of Agricultural Hydraulics, University of Milan, via Celoria no.2, Milan 20133, Italy*

Abstract

The study of droplet evaporation is applied to many and varied fields: the present approach is oriented to sprinkler irrigation. This paper examines a parametric study on the evaporation in air of a single droplet, with the aim of highlighting the influence of each parameter alone on the evaporative process. Four parameters are investigated: air temperature, droplet initial velocity, droplet initial diameter, diffusion coefficient of vapour in air. Droplet evaporation is studied through numerical-CFD simulation employing STAR-CCM+ version 5.04.012 software, which treats the evaporative phenomenon hypothesizing quasi-steady conditions, given the interface low liquid-gas vapour concentration gradients. The results are provided as time- and space-dependent in-percentage evaporation rates, the latter ones after defining a specific distance, from the injection point, to be covered. Apart from a qualitatively predictable effect of air temperature and diffusion coefficient of vapour in air, droplet initial velocity and above all droplet initial diameter prove not at all to be negligible when managing an irrigation process, the latter being inversely proportional to droplet mass evaporation. These results prove that droplet evaporation is a complicate fluid dynamic effect and cannot be simply regarded as a diffusive process. The final discussion provides some practical remarks useful to irrigation operators.

Introduction

Droplet evaporation is thoroughly investigated [1-4] as it is applied to multivarious engineering fields like automotive [5-15], air-conditioning [16,17], fluidized beds [18], fire suppression [19], geophysics [20], meteorology [21] and agriculture [3,4,22-28]. In the latter case the focus is on irrigation systems, whose design for both civil and agricultural use must consider, within a sustainable economy context, the worrying depletion of an important resource: water. As a matter of fact, during irrigation the single water particles come in contact with air and evaporate: this is to be attributed to many parameters, among which are those that will be here considered, i.e. air-water temperature difference, droplet initial velocity, droplet initial diameter and diffusion coefficient of vapour in air. Several studies, both experimental and theoretical [3,4,26,27,29-37], were carried out in the past in order to quantify evaporation loss. As regards the second type, a "classic" approach was that by Kinzer and Gunn [29], who modelled evaporation for falling droplets but neglected the dynamics acting upon the in-flight droplets; they arrived at the following expression, suitable for a limited Reynolds number range:

$$m^{\wedge} = 4 \, \pi \, a^2 \, D_{va} G$$

where: $m^{\wedge}$ [kg s^{-1}] is droplet mass evaporated with time, a [m] is its radius; D_{va} [m^2 s^{-1}] is diffusion coefficient of vapour in air and G [kg m^{-4}] is the vapour-density gradient established at the surface of the droplet. Also Ranz and Marshall [30,31] described in-flight droplet evaporation with an equation for molecular transfer rate, which was modified by Goering et al. [38], who used empirical formulae even from other authors:

$$D^{\wedge} = -2 \, M^{\wedge} \, K^{\wedge} \, R \, P \, Nu^{*}$$

where: $D^{\wedge}$ [m s^{-1}] is droplet diameter variation with time; $M^{\wedge}$ [-] is the ratio between molecular weights of vapour and air; $K^{\wedge}$ [m s^{-1}] is the ratio between D_{va} [m^2 s^{-1}] and d_p [m]; R [-] is the ratio between air and droplet density; P [-] is the ratio: difference between saturation pressure at wet bulb air temperature and vapour pressure at dry bulb temperature / partial pressure of air; and Nu* [-] is a specially defined Nusselt number for mass transfer. Still on theoretical approaches, a simplified mathematical model, validated by experimental data, was developed by Lorenzini and applied to the case studies examined by Edling [22] and Thompson et al. [23] for comparison purposes [3,4,27,28]. There is a strong correlation among the chemical-physical processes that characterize the evolution of sprays and an analytical model attempting at this description may be strongly conditioned in arriving at a closed-form solution by the non-linear nature of the partial differential equations arising. A further step in literature was taken thanks to CFD implementation [13,39-43], even though most of the researches were applied to the field of combustion rather than to agricultural sprays and this makes the temperature and chemical context quite far from that here faced, so considering even high values of the Spalding Number which, on the contrary, did not happen in this study. The present paper analyses the evolution, alternatively with time or with space (i.e. for a simulation time equal to 4 s or for a simulation path of 20 m from the injection point, where a suitable check-plane was located), of the evaporative phenomenon in air of a single water droplet. Phenomenon modelling and solving were performed by means of the CFD control volume code STAR-CCM+ version 5.04.012. Treatment included a straight droplet trajectory defined downwards along the vertical axis

*Corresponding author: Daniele De Wrachien, University of Milan, Department of Agricultural Hydraulics, via Celoria no.2, Milan 20133, Italy, E-mail: daniele.dewrachien@unimi.it

and not affected neither by wind action nor by solar radiation. The present parametric study included the following variables: droplet initial velocity; droplet initial diameter; air temperature; and diffusion coefficient of vapour in air. Air relative humidity, a parameter which is indeed relevant to the whole phenomenological picture, was instead not considered here due to technical limits, because the solver implemented within STAR CCM+ could not tackle that issue due to a water-air interface modelling limit: this, anyway, does not affect the generality of the present study as the "classical" parametric approach adopted (one variable varying at a time for every simulation; all the others kept as constants) assures the independence of any parametric result from another. Droplet evaporation was described by means of an Eulerian-Lagrangian approach, typical of this kind of processes [44,45], even if fully Lagrangian approaches [46] and other approaches [47] are also reported in literature. A range of twenty cases study was faced, five for each analysis parameter.

Method

The simulations performed involve the evaporation of a single water droplet into the air, considering the influence of four physical parameters (air temperature, diffusion coefficient of vapour in air; droplet initial velocity and droplet initial diameter): the aim is to examine a dynamically realistic process, also accounting for the contribution of air friction to evaporation [4]. Simulations involve the investigation and determination of the evaporation rate of a liquid particle moving vertically downwards; such particle, located within the control volume, starts its path at a given set of initial conditions. Friction and gravity are the forces influencing the system and are opposite to one another, directed along the x axis as Figure 1 displays together with a detail of the meshed domain. The numerical modelling of the phenomenon was carried out adopting an Eulerian-Lagrangian approach, in which a Lagrangian phase (water droplet) moves within a continuous Eulerian phase (air). Liquid particles are rigid spheres, hence the simulations do not consider the degree of deformation caused by air friction and undergone by a droplet along its path: previous researches demonstrated this assumption to be satisfactory and realistic [48,49]. The numerical approach employed by STAR-CCM+ version 5.04.012 does not model the liquid-gas interface directly, but solves it defining the diffusion law at the interface (Fick's law). All the simulations were unsteady, given the intrinsic dependence of unsaturated evaporation upon time [50]. Physical properties of air and water were taken by the STAR-CCM+ version 5.04.012 code library; the same for the values of the constants in the relations presented below (for example, the Sutherland's or Antoine's laws). Sutherland's law was adopted for air viscosity μ_a [Pa s] [51,52]:

$$\mu_a = \mu_0 \cdot \frac{T_0 + 111}{T_a + 111} \cdot \left(\frac{T_a}{T_0}\right)^{\frac{3}{2}} \tag{1}$$

in which μ_0 (dynamic viscosity at the temperature T_0) is equal to 1.716 $\times 10^{-5}$ Pa s, $T_0 = 273.15$ K, and T_a [K] is the air temperature. Antoine's law was used for computing the saturation pressure and hence the vapour tension [52,53]:

$$p_{sat} = p_{atm} exp\left(A - \frac{B}{T - C}\right) \tag{2}$$

in which T [K] is temperature, p_{atm} is equal to atmospheric pressure (= 1 atm), A = 11.949; B = 3978.205 and C = -39.801 [52]. Friction force has the following expression, valid just in case of a no-wind condition:
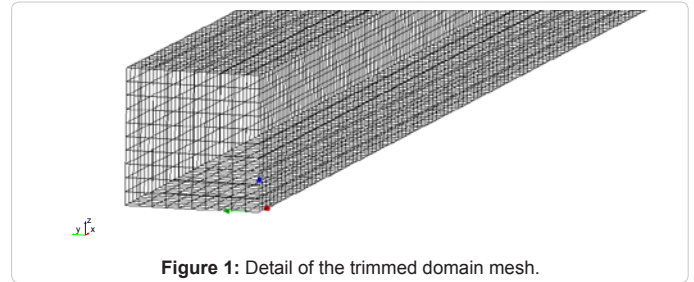

Figure 1: Detail of the trimmed domain mesh.

$$\vec{F}_d = \frac{1}{2} \cdot C_d \cdot \rho_a \cdot A_p \cdot \vec{v}_p \cdot |v_p| \tag{3}$$

Where C_d [-] is the friction factor, ρ_a [kg m^{-3}] is air density, A_p [m^2] is droplet cross sectional area and v_p [m s^{-1}] is velocity of the Lagrangian phase. The code employs Schiller-Naumann law for calculating the friction factor [54]:

$$C_d = \begin{cases} \frac{24}{Re_p} \cdot \left(1 + 0.15 \cdot Re_p^{0.687}\right) & Re_p \leq 1000 \\ 0.44 & Re_p \geq 1000 \end{cases} \tag{4}$$

Evaporation is a phenomenon directly connected with energy, hence it involves the heat exchange coefficients, namely the Nusselt number (here called Nu_p [-] as referred to the water particle). The Ranz-Marshall correlation was used for calculating the heat transfer coefficients during evaporation and has to be retained valid for spherical droplets up to $Re_p \approx 5000$ [30,31]:

$$Nu_p = 2 + 0.6 \cdot Re_p^{\frac{1}{2}} \cdot Pr_a^{\frac{1}{3}} \tag{5}$$

Where the Prandtl number Pr_a [-] refers to the gas phase (air) and the Reynolds number of the droplet Re_p [-] is defined as follows:

$$Re_p = \frac{\rho_a \cdot v_p \cdot d_p}{\mu_a} \tag{6}$$

in which ρ_a [kg m^{-3}] is air density, μ_a [Pa s] is air viscosity, d_p [m] is droplet diameter and v_p [m s^{-1}] is water particle velocity. Air density and viscosity are calculated at the mean temperature between those of air (T_a [K]) and water (T_w [K]) as: $[(T_a + T_w)/2]$ [55]. It has to be specified that temperature gradients within a droplet have not been analysed here, as Biot numbers throughout the investigation proved to be always very close to zero thus making it reasonable, in a just-evaporative investigation, to consider the droplet itself as isothermal. About recirculation in droplets: this is an important issue but we feel it more as a possible further development of the current research (based on comprehensive droplet evaporation assessment and not on a punctual thermal fluid dynamic analysis of the transient process) rather than a detail of the present work.

In this study the diffusion coefficient of vapour in air D_{va} [m^2 s^{-1}], which essentially depends upon many factors (e.g.: temperature, air pressure, vapour pressure gradient), is kept constant throughout the simulation duration; its values can be calculated in different ways: through both theoretical [56] and semi-empirical formulas [57-60], and through tabulated values found in literature [53,55,61]. In this investigation the diffusion coefficients were first calculated according

to the former way (formulas) and then compared to the latter one (tabulated values), identifying an interval between 0.2×10^{-4} m^2 s^{-1} and 0.3×10^{-4} m^2 s^{-1} as realistic within the analysis parameters range tested. Schmidt number Sc [-] and Sherwood number Sh [-] are both connected to the diffusion coefficient D_{va} [m^2 s^{-1}]. Sh number can be expressed in function of Re [-] and Sc [-]. In the case studies tackled here, being the droplet spherical, Ranz-Marshall expression can be employed [30,31]:

$$Sh = 2 + 0.6 \cdot Re_p^{\frac{1}{2}} \cdot Sc^{\frac{1}{3}} \qquad (7)$$

being this expression analogous to equation (5), with Re_p [-] calculated according to equation (6). In-percentage droplet mass evaporation rate Δm [%] is defined as follows:

$$\ddot{A}m = \frac{m_0 - m_1}{m_0} \cdot 100 \qquad (8)$$

where m_0 [kg] represents the droplet initial mass and m_1 [kg] the mass observed at a dimensionless time t* defined as:

$$t* = \frac{t}{t_{max}} \qquad (9)$$

in which t [s] is the variable time and t_{max} [s] is the maximum simulation time (4 s). Alternatively, a target location placed at set distance (20 m) from the droplet injection point is considered and Δm [%] is checked there. This choice will add significant insight to the present study, as the Discussion section will explain. To add generality to the approach it has been defined a dimensionless travel distance L* [-]:

$$L* = \frac{L}{L_{max}} \qquad (10)$$

Where L [m] is travel distance and L_{max} = 20 m is the target location just above defined, reached after a simulation time of t_{Lmax} [s] which is made dimensionless ($t*_{Lmax}$ [-]) as it follows:

$$t*_{Lmax} = \frac{t_{Lmax}}{t_{max}} \qquad (11)$$

Parameters and Boundary Conditions

The study is a parametric one: all the parameters, except one kept constant during each test, were kept constant throughout the simulation. The following analysis parameters were considered:

air temperature (T_a [K]);

droplet initial velocity (v_i [m s^{-1}]);

diffusion coefficient of vapour in air (D_{va} [m^2 s^{-1}]);

droplet initial diameter (d_i [m]).

Table 1 reports the whole set of analysis parameters and cases study faced in the present investigation. In relation to T_a [K], five values were chosen within an interval range compatible with the climatic conditions of a hot-arid environment: 300 K, 305 K, 310 K, 315 K and 320 K. Whereas, droplet initial velocities and diameters were selected among typical values of a wide range of sprinkler systems [62,63]. The diffusion coefficient of vapour in air D_{va} [m^2 s^{-1}] is a rather important parameter in the dynamics of evaporation as it is directly connected to the vapour film which envelopes water droplets: its range of variation was determined, as explained in the previous section of this paper, comparing computed to tabulated data in relation to the general conditions of the tests performed. As explained in the previous

section, after comparing computed to tabulated data the range of D_{va} [m^2 s^{-1}] investigated was $0.2 \times 10^{-4} \div 0.3 \times 10^{-4}$ m^2 s^{-1} [53,55,56-61], choosing in detail the following test values: 0.2×10^{-4} m^2 s^{-1}, 0.225×10^{-4} m^2 s^{-1}, 0.25×10^{-4} m^2 s^{-1}, 0.275×10^{-4} m^2 s^{-1} and 0.3×10^{-4} m^2 s^{-1}. The droplet velocity is directly connected to the friction force (a quadratic function of it) [55], which plays a significant role in the process under exam [4,27]. To gather direct information on its effect five ascending values of v_i [m s^{-1}] were investigated: 1 m s^{-1}, 5 m s^{-1}, 15 m s^{-1}, 25 m s^{-1} and 30 m s^{-1}. Finally, as droplet evaporation also depends on the droplet diameter, five values of d_i [m] were tested, within the typical range $0.001 \div 0.003$ m [62-66]: 0.001 m, 0.0015 m, 0.002 m, 0.0025 m and 0.003 m. Water temperature T_w [K] was a constant and kept equal to 288 K throughout the investigation. The simulations were performed in unsteady state, given the intrinsic nature of evaporation under conditions far from saturation, and the path followed by the liquid particle within the control volume was alternatively observed at t* = 1 or L* = 1, as explained above.

Numerical Settings

The numerical domains based on control volume approach are geometrically simple: they are in fact represented by parallelepiped volumes and in this study their dimensions are identical in all cases study but those where the droplet initial diameter was the parameter tested (Table 2). In the latter cases the geometric dimensions of the computational domain were variable from one case to another along the droplet path direction (x-axis in Figure 1), while dimensions along z- and y-axes remained unchanged. Table 2 summarises the geometrical dimensions of all the domains tested, in addition to the main numerical settings. Given the extremely simple geometry, the mesh for the numerical domain is of the "trimmed" type (see detail

Cases study	Analysis parameters				Constant
	v_i [m s^{-1}]	d_i [m]	D_{va} [m^2 s^{-1}]	T_a [K]	T_w [K]
Case 1	1	0.001	0.3×10^{-4}	320	288
Case 2	5	0.001	0.3×10^{-4}	320	288
Case 3	15	0.001	0.3×10^{-4}	320	288
Case 4	25	0.001	0.3×10^{-4}	320	288
Case 5 (*)	30	0.001	0.3×10^{-4}	320	288
Case 6 (*)	30	0.001	0.3×10^{-4}	320	288
Case 7	30	0.0015	0.3×10^{-4}	320	288
Case 8	30	0.002	0.3×10^{-4}	320	288
Case 9	30	0.0025	0.3×10^{-4}	320	288
Case 10	30	0.003	0.3×10^{-4}	320	288
Case 11	30	0.001	0.2×10^{-4}	320	288
Case 12	30	0.001	0.225×10^{-4}	320	288
Case 13	30	0.001	0.25×10^{-4}	320	288
Case 14	30	0.001	0.275×10^{-4}	320	288
Case 15 (*)	30	0.001	0.3×10^{-4}	320	288
Case 16	30	0.001	0.3×10^{-4}	300	288
Case 17	30	0.001	0.3×10^{-4}	305	288
Case 18	30	0.001	0.3×10^{-4}	310	288
Case 19	30	0.001	0.3×10^{-4}	315	288
Case 20 (*)	30	0.001	0.3×10^{-4}	320	288

Table 1: Analysis parameters and cases study (those marked with * are duplicated). The numbers reported are input data and they consequently represent exact numbers.

Cases study	Time step [s]	x-axis [m]	y-axis [m]	z-axis [m]	Mesh [m]	Number of cells	Number of faces
Case 1	1×10^{-2}	25	1×10^{-1}	1×10^{-1}	5×10^{-3}	845 952	2 472 540
Case 2	5×10^{-3}	25	1×10^{-1}	1×10^{-1}	5×10^{-3}	845 952	2 472 540
Case 3	1.5×10^{-3}	25	1×10^{-1}	1×10^{-1}	5×10^{-3}	845 952	2 472 540
Case 4	5×10^{-4}	25	1×10^{-1}	1×10^{-1}	5×10^{-3}	845 952	2 472 540
Case 5 (*)	3×10^{-4}	25	1×10^{-1}	1×10^{-1}	5×10^{-3}	845 952	2 472 540
Case 6 (*)	3×10^{-4}	25	1×10^{-1}	1×10^{-1}	5×10^{-3}	845 952	2 472 540
Case 7	7.5×10^{-4}	30	1×10^{-1}	1×10^{-1}	1×10^{-2}	300 000	839 900
Case 8	7.5×10^{-4}	35	1×10^{-1}	1×10^{-1}	1×10^{-2}	350 000	979 900
Case 9	7.5×10^{-4}	40	1×10^{-1}	1×10^{-1}	1×10^{-2}	400 000	1 119 900
Case 10	1×10^{-3}	45	1×10^{-1}	1×10^{-1}	1.2×10^{-2}	247 442	674 817
Case 11	3×10^{-4}	25	1×10^{-1}	1×10^{-1}	5×10^{-3}	845 952	2 472 540
Case 12	3×10^{-4}	25	1×10^{-1}	1×10^{-1}	5×10^{-3}	845 952	2 472 540
Case 13	3×10^{-4}	25	1×10^{-1}	1×10^{-1}	5×10^{-3}	845 952	2 472 540
Case 14	3×10^{-4}	25	1×10^{-1}	1×10^{-1}	5×10^{-3}	845 952	2 472 540
Case 15 (*)	3×10^{-4}	25	1×10^{-1}	1×10^{-1}	5×10^{-3}	845 952	2 472 540
Case 16	3×10^{-4}	25	1×10^{-1}	1×10^{-1}	5×10^{-3}	845 952	2 472 540
Case 17	3×10^{-4}	25	1×10^{-1}	1×10^{-1}	5×10^{-3}	845 952	2 472 540
Case 18	3×10^{-4}	25	1×10^{-1}	1×10^{-1}	5×10^{-3}	845 952	2 472 540
Case 19	3×10^{-4}	25	1×10^{-1}	1×10^{-1}	5×10^{-3}	845 952	2 472 540
Case 20 (*)	3×10^{-4}	25	1×10^{-1}	1×10^{-1}	5×10^{-3}	845 952	2 472 540

Table 2: Computational domain details and numerical settings (the cases marked with * are those duplicated). The numbers reported are input data and they consequently represent exact numbers.

Cases study	Δm [%]	m_0 [kg]	m_1 [kg]
Case 1	7.8116%	5.2232×10^{-7}	4.8152×10^{-7}
Case 2	8.0567%	5.2232×10^{-7}	4.8024×10^{-7}
Case 3	8.3400%	5.2232×10^{-7}	4.7876×10^{-7}
Case 4	8.4874%	5.2232×10^{-7}	4.7799×10^{-7}
Case 5 (*)	8.5755%	5.2232×10^{-7}	4.7753×10^{-7}
Case 6 (*)	8.5755%	5.2232×10^{-7}	4.7753×10^{-7}
Case 7	5.2412%	1.7628×10^{-6}	1.6704×10^{-6}
Case 8	3.6905%	4.1785×10^{-6}	4.0244×10^{-6}
Case 9	2.7776%	8.1612×10^{-6}	7.9346×10^{-6}
Case 10	2.1841%	1.4102×10^{-5}	1.3795×10^{-5}
Case 11	7.4287%	5.2232×10^{-7}	4.8352×10^{-7}
Case 12	7.7431%	5.2232×10^{-7}	4.8188×10^{-7}
Case 13	8.0301%	5.2232×10^{-7}	4.8038×10^{-7}
Case 14	8.2925%	5.2232×10^{-7}	4.7901×10^{-7}
Case 15 (*)	8.5755%	5.2232×10^{-7}	4.7753×10^{-7}
Case 16	6.1574%	5.2232×10^{-7}	4.9016×10^{-7}
Case 17	6.7168%	5.2232×10^{-7}	4.8724×10^{-7}
Case 18	7.3015%	5.2232×10^{-7}	4.8418×10^{-7}
Case 19	7.9084%	5.2232×10^{-7}	4.8101×10^{-7}
Case 20 (*)	8.5755%	5.2232×10^{-7}	4.7753×10^{-7}

Table 3: Results computed at $t^* = 1$ (the cases marked with * are those duplicated). The numbers reported in the third and fourth columns are numerical results and their representation respect the criterion of significant figures homogeneity; the numbers in the second column are computed values and respect the criterion of decimal figures homogeneity.

in Figure 1): the hexagonal three-dimensional elements are arranged (cut and connected) to form a mesh made up of cubic elements. Their side was kept constant and equal to 0.005 m (apart from those case studies where the droplet initial diameter effect was assessed), while the time step varied in function of v_i [m s^{-1}], as highlighted in Table 2, decreasing as velocity increases (in order to achieve a suitable "resolution" of the physical phenomenon) and increasing with d_i [m] for numerical reasons related to convergence of the solution. By adopting an Eulerian-Lagrangian approach, the code STAR-CCM+

version 5.04.012 requires some bonds to be respected, for the internal subsistence of such approach [52]. In detail, the volume fraction occupied by the Lagrangian phase in a single cell must be lower than 0.01. For such reason in Cases from 7 to 10, in which droplet diameter d_i [m] varied from 0.0015 to 0.003 m (see Table 1), the mesh dimensions were increased and the cells were assigned a side of 0.01 or 0.012 m.

Results

The evaporation process involving a water droplet moving through the air is influenced by a wealth of factors. This paper deals with the importance of four among the most important influencing factors: droplet initial velocity, air temperature, diffusion coefficient of vapour in air and droplet initial diameter. In the figures displaying the evaporation rate trend, calculated according to eq. 8, it was made possible an analysis comparing the temporal-dependent and spatial-dependent homologous results, as already stated, setting a simulation time $t^* = 1$, on the one hand, and a dimensionless travel distance $L^* = 1$, on the other. Hereafter each case study (except those duplicated) is considered one at a time to reach a clear picture of the results arrived at. Tables 3 and 4 showcase the main evaporation results at $t^* = 1$ and $L^* = 1$, respectively.

Velocity is the first analysis parameter considered (Case 1 to Case 5).

Case 1 ($v_i = 1$ m s^{-1})

This case studies evaporation of a single water droplet which leaves an irrigation sprinkler nozzle with velocity of 1 m s^{-1}. The thermophysical conditions of water and air are reported in Table 1. At $t^* = 1$ one gets an in-percentage mass evaporation rate of 7.8116% (Table 3); while fixing an ideal plane perpendicular to the droplet direction and located at $L^* = 1$ gives an in-percentage mass evaporation rate of 10.4416% (Table 4) as the droplet reaches that set position at $t^*_{Lmax} = 1.3375$ (Table 4).

Case 2 ($v_i = 5$ m s^{-1})

Here it is tackled the case of a single water droplet (evaporating)

characterised by an initial velocity of 5 m s^{-1}. The thermophysical conditions of water and air are reported in Table 1. Considering t* = 1 one computes an in-percentage evaporation rate of 8.0567% (+0.2451% with respect to Case 1), as reported in Table 3. This datum gives the first signal that higher velocity may cause bigger evaporation rates: drag force, which depends on velocity according to eq. 3, affects the evaporation phenomenon. By fixing a target plane perpendicular to droplet path and located at L* = 1, the droplet reaches that ideal plane at t*$_{Lmax}$ = 1.2594 (Table 4), where an evaporation rate of 10.1278% is computed (-0.3138% with respect to Case 1, as t*$_{Lmax}$ [-] is now smaller because of a higher velocity).

Case 3 (v$_i$ = 15 m s^{-1})

This case studies the evaporation of a single water droplet leaving an irrigation sprinkler nozzle with initial velocity of 15 m s^{-1}. The thermophysical conditions of water and air are reported in Table 1. If one considers a dimensionless time t* = 1, the related in-percentage mass evaporation rate is equal to 8.3400% (Table 3). With respect to Case 1 (+0.5284%) and Case 2 (+0.2833%) this result confirms proportionality between evaporation and velocity, which may be ascribed to the drag force as strictly related to velocity (eq. 3). Checking the space-dependent evaporation result (i.e. for a dimensionless travel distance of L* = 1), the droplet flight lasts t*$_{Lmax}$ = 1.1511 (Table 4) and determines an evaporation rate equal to 9.6572% (Table 4). The latter datum is proves smaller than those in both Case 2 (-0.4706%) and Case 1 (-0.7844%), being t*$_{Lmax}$ lower in this case due to an augmented droplet initial velocity.

Case 4 (v$_i$ = 25 m s^{-1})

This case relates to the evaporation process occurring to a water droplet with velocity of 25 m s^{-1}. The thermophysical conditions of water and air are reported in Table 1. After a simulation time of t* = 1 the in-percentage evaporation rate of 8.4874% is arrived at (Table 3). With respect to Case 1 (+0.6758 %), Case 2 (+0.4307%) and Case 3 (+0.1474%) the higher velocity – higher evaporation trend proves its consistency and confirms the air friction effect in affecting evaporation. After a dimensionless travel distance of L* = 1 (corresponding to a simulation time t*$_{Lmax}$ = 1.0728, see Table 4) in-percentage evaporation rate becomes 9.0927% (Table 4): this value, as it may now be expected, is less than those of Case 1 (-1.3489%), Case 2 (-1.0351%) and Case 3 (-0.5645%) because of t*$_{Lmax}$ decrease.

Case 5 (v$_i$ = 30 m s^{-1})

In this case the initial droplet velocity is the highest tested: 30 m s^{-1}. The thermophysical conditions of water and air are reported in Table 1. Once reached a time dimensionless value of t* = 1, the in-percentage evaporation rate of 8.5755% is reached (Table 3). With respect to Case 1 (+0.7639%), Case 2 (+0.5188%), Case 3 (+0.2355%) and Case 4 (+0.0881%) the same parametrical trend is confirmed: higher velocities cause higher evaporation as air friction characterises the process (see also eq.3). If the spatial effect, instead, is considered: once reached a distance L* = 1 (which happens at t*$_{Lmax}$ = 1.0399, see Table 4), an evaporation rate equal to 8.8496% (Table 4) is arrived at. This figure is lower than those of Case 1 (-1.5920%), Case 2 (-1.2782%), Case 3 (-0.8076%) and Case 4 (-0.2431%), again because of the role played by t*$_{Lmax}$ as related to velocity.

Initial droplet diameter is the second analysis parameter considered (Case 6 to Case 10).

Case 6 (d$_i$ = 0.001 m)

See Case 5 (duplicated case: the combination of the analysis parameters considered, leads case 6 to be coincident with case 5).

Case 7 (d$_i$ = 0.0015 m)

In this case study it is investigated the evaporation of a single water droplet with initial diameter of 0.0015 m. The thermophysical conditions of water and air are reported in Table 1. At the dimensionless instant of time t* = 1 the corresponding in-percentage evaporation rate is 5.2412% (-3.3343% with respect to Case 6), as shown in Table 3. This datum shows that a bigger droplet diameter results in a lower evaporation rate: this may be credited to an augmented thermal inertia which tends to limit evaporation and to a decreased surface over volume ratio, reducing the diffusion of vapour in air in relation to the volume of the drop. At the dimensionless travel distance L* = 1 from inlet, which the droplet covers after a dimensionless time t*$_{Lmax}$ = 0.6746 (Table 4), the evaporation rate is 3.6569% (-5.1927% with respect to Case 6, due to a reduction in t*$_{Lmax}$ creditable to an increase in gravity), as Table 4 shows.

Case 8 (d$_i$ = 0.002 m)

The present case tackles in-flight droplet evaporation when an initial diameter of 0.002 m is set. The thermophysical conditions of water and air are reported in Table 1. An in-percentage evaporation rate of 3.6905% (Table 3) is arrived at after the time dimensionless co-ordinate t* has reached a value equal to 1. With respect to Case 6 (-4.8850%) and Case 7 (-1.5507%) it may be evicted that increasing the initial diameter means decreasing the evaporation rate: increased droplet thermal inertia and decreased surface over volume ratio may be pointed out as responsible for that. Parallel, an in-percentage evaporation rate of 2.0061% (Table 4) is computed considering a dimensionless covered

Cases study	Δm [%]	m$_0$ [kg]	m$_1$ [kg]	t*$_{Lmax}$ [-]
Case 1	10.4416	5.2232 × 10^{-7}	4.6795 × 10^{-7}	1.3375
Case 2	10.1278	5.2232 × 10^{-7}	4.6942 × 10^{-7}	1.2594
Case 3	9.6572	5.2232 × 10^{-7}	4.7188 × 10^{-7}	1.1511
Case 4	9.0927	5.2232 × 10^{-7}	4.7483 × 10^{-7}	1.0728
Case 5 (*)	8.8496	5.2232 × 10^{-7}	4.7610 × 10^{-7}	1.0399
Case 6 (*)	8.8496	5.2232 × 10^{-7}	4.7610 × 10^{-7}	1.0399
Case 7	3.6569	1.7628 × 10^{-6}	1.6984 × 10^{-6}	0.6746
Case 8	2.0061	4.1785 × 10^{-6}	4.0947 × 10^{-6}	0.5111
Case 9	1.2975	8.1612 × 10^{-6}	8.0554 × 10^{-6}	0.4336
Case 10	0.9165	1.4102 × 10^{-5}	1.3973 × 10^{-5}	0.3824
Case 11	7.6981	5.2232 × 10^{-7}	4.8211 × 10^{-7}	1.0375
Case 12	8.0237	5.2232 × 10^{-7}	4.8041 × 10^{-7}	1.0381
Case 13	8.3221	5.2232 × 10^{-7}	4.7885 × 10^{-7}	1.0387
Case 14	8.5954	5.2232 × 10^{-7}	4.7743 × 10^{-7}	1.0393
Case 15 (*)	8.8496	5.2232 × 10^{-7}	4.7610 × 10^{-7}	1.0399
Case 16	6.5243	5.2232 × 10^{-7}	4.8824 × 10^{-7}	1.0728
Case 17	7.0826	5.2232 × 10^{-7}	4.8533 × 10^{-7}	1.0641
Case 18	7.6578	5.2232 × 10^{-7}	4.8232 × 10^{-7}	1.0558
Case 19	8.2470	5.2232 × 10^{-7}	4.7925 × 10^{-7}	1.0476
Case 20 (*)	8.8496	5.2232 × 10^{-7}	4.7610 × 10^{-7}	1.0399

Table 4: Results computed at L* = 1 (the cases marked with * are those duplicated). The numbers reported in the third and fourth columns are numerical results and their representation respect the criterion of significant figures homogeneity; the numbers in the second column are computed values and respect the criterion of decimal figures homogeneity.

distance $L^* = 1$ (at $t^*_{Lmax} = 0.5111$, see Table 4): such value, smaller than those of both Case 6 (-6.8435%) and Case 7 (-1.6508%) confirms the trend previously highlighted.

Case 9 ($d_i = 0.0025$ m)

This case takes into account the aerial evaporation of a single water droplet with initial diameter of 0.0025 m. The thermophysical conditions of water and air are reported in Table 1. If one considers a dimensionless time interval $t^* = 1$, the simulation provides an in-percentage evaporation rate of 2.7776% (Table 3). With respect to Case 6 (-5.7979%), Case 7 (-2.4636%) and Case 8 (-0.9129%) the general trend is confirmed, i.e. an increased droplet diameter causes a decrement in the evaporation rate. Augmented droplet thermal inertia and diminished surface over volume ratio are the reasons for that. Considering instead a dimensionless travel distance $L^* = 1$, covered in a dimensionless time $t^*_{Lmax} = 0.4336$ (Table 4), it is obtained an in-percentage evaporation rate of 1.2975% (Table 4), smaller than that of Case 6 (-7.5521%), Case 7 (-2.3594%) and Case 8 (-0.7086%) for the same physical and mechanical reasons explained above.

Case 10 ($d_i = 0.003$ m)

The present case study is about an evaporating droplet with initial diameter of 0.003 m. The thermophysical conditions of water and air are reported in Table 1. Considering $t^* = 1$: in-percentage evaporation rate is 2.1841% (Table 3). Comparing such figure to the previous cases one has: Case 6 (-6.3914%); Case 7 (-3.0571%); Case 8 (-1.5064%); and Case 9 (-0.5935%). This completes the whole picture examined proving that augmenting a diameter acts upon two significant parameters: thermal inertia (increasing it) and surface over volume ratio (decreasing it). Both these variations tend to limit evaporation. Same considerations may be made considering a spatial targeting of the analysis: $L^* = 1$ (for $t^*_{Lmax} = 0.3824$, see Table 4). In-percentage evaporation rate becomes 0.9165% (Table 4), being the figure smaller than in Case 6 (-7.9331%), Case 7 (-2.7405%), Case 8 (-1.0896%) and Case 9 (-0.3810%).

Diffusion coefficient of water vapour in the air is the third analysis parameter considered (Case 11 to Case 15).

Case 11 ($D_{va} = 0.2 \times 10^{-4}$ m^2 s^{-1})

In this case study it is investigated the evaporation of a single water droplet when D_{va} is set equal to 0.2×10^{-4} m^2 s^{-1}. The thermophysical conditions of water and air are reported in Table 1. At the dimensionless instant of time $t^* = 1$ the corresponding in-percentage evaporation rate is 7.4287%, as shown in Table 3. At the dimensionless travel distance $L^* = 1$ from inlet, which the droplet covers after a dimensionless time $t^*_{Lmax} = 1.0375$ (Table 4), the evaporation rate is 7.6981%, as Table 4 shows.

Case 12 ($D_{va} = 0.225 \times 10^{-4}$ m^2 s^{-1})

This test studies single droplet evaporation in case of a diffusion coefficient value of 0.225×10^{-4} m^2 s^{-1}. The thermophysical conditions of water and air are reported in Table 1. When $t^* = 1$, the in-percentage evaporation rate becomes equal to 7.7431%, as shown in Table 3. Compared to the previous case (Case 11) evaporation results to be increased by a 0.3144 percentage, easily (from a qualitative point of view) explainable as increasing D_{va} tends to favour evaporation (when all the other parameters are kept constant). Instead, when $L^* = 1$ (i.e. at $t^*_{Lmax} = 1.0381$, see Table 4) in-percentage droplet mass evaporation is equal to 8.0237% (Table 4). This figure is higher than in Case 11 (0.3256%), confirming, on the one hand, a direct proportionality

between diffusion coefficient, on the other, the correct predictions obtainable by the code.

Case 13 ($D_{va} = 0.25 \times 10^{-4}$ m^2 s^{-1})

A D_{va} value of 0.25×10^{-4} m^2 s^{-1} is here considered to check its effect on a single droplet evaporation. Again, the thermophysical conditions of water and air are reported in Table 1. In the present case the in-percentage mass evaporation rate at dimensionless time $t^* = 1$ is equal to 8.0301% (Table 3). If compared to Case 11 and Case 12, as qualitatively expectable, there is an evaporation augmentation of +0.6014% and +0.2870%, respectively, due to the modified diffusion coefficient value which enhances the process. By considering evaporation after a dimensionless travel distance equal to $L^* = 1$ (covered in $t^*_{Lmax} = 1.0387$, see Table 4), the evaporation result is equal to 8.3221% (Table 4): this datum is higher than in both Case 11 (+0.6240%) and Case 12 (+0.2984%), as the time of flight is higher in relation to the effect of gravity.

Case 14 ($D_{va} = 0.275 \times 10^{-4}$ m^2 s^{-1})

Case 14 faces droplet evaporation when the diffusion coefficient of vapour in air is set equal to 0.275×10^{-4} m^2 s^{-1} (thermophysical conditions of water and air are available in Table 1). The mass evaporation in-percentage figure results 8.2925% at $t^* = 1$ (Table 3). Compared to the previous cases (Case 11, Case 12, Case 13) the same trend is confirmed, showing an augmentation of +0.8638%, +0.5494% and +0.2624, respectively, being an increase of D_{va} [m^2 s^{-1}] in favour of a more intense evaporation. Moreover, if a dimensionless travel distance $L^* = 1$ is covered by the droplet after a time of $t^*_{Lmax} = 1.0393$ (Table 4), then a mass droplet evaporation of 8.5954% is arrived at (Table 4). The latter datum is, again, part of the increasing trend examined in the previous cases: it boasts a +0.8973%, +0.5717% and +0.2733% with respect to Cases 11, 12, and 13, respectively.

Case 15 ($D_{va} = 0.3 \times 10^{-4}$ m^2 s^{-1})

See Case 5 (duplicated case: the combination of the analysis parameters considered, leads case 15 to be coincident with case 5).

Air temperature is the last parameter here investigated (Case 16 to Case 20).

Case 16 ($T_a = 300$ K)

This case study is about droplet evaporation in case of surrounding air at a temperature of 300 K. The thermophysical conditions of water and air are, again, reported in Table 1. As Table 3 displays, the in-percentage mass evaporation rate after a dimensionless time of $t^* = 1$ is equal to 6.1574%; while after a dimesionless distance $L^* = 1$ (covered after a time interval $t^*_{Lmax} = 1.0728$, see Table 4) a droplet mass percentage of 6.5243% is evaporated (Table 4).

Case 17 ($T_a = 305$ K)

It is here considered an air temperature of 305 K (thermophysical conditions of water and air are in Table 1) and its effect on a single droplet aerial evaporation. At $t^* = 1$ the mass evaporation figure is of 6.7168% (Table 3), that is +0.5594% with respect to Case 16 as an augmented air temperature, keeping all the other parameters constant, plays in favour of an increased evaporation. By setting a dimensionless travel distance of $L^* = 1$ (covered after $t^*_{Lmax} = 1.0641$, see Table 4), droplet mass evaporation becomes equal to 7.0826% (Table 4), i.e. higher than in Case 16 (+0.5583%).

Case 18 (T_a = 310 K)

This case studies droplet evaporation when the surrounding air is at 310 K. The thermophysical conditions of water and air are reported in Table 1. At t* = 1 the computed mass evaporation is equal to 7.3015% (Table 3): +1.1441% and +0.5847% compared to Case 16 and Case 17, respectively, which can be explained as increasing the temperature of the medium into which the droplet flows makes its evaporation more intense. Considering instead the spatial effect of air temperature, i.e. L* = 1 (at t^*_{Lmax} = 1.0558, see Table 4), mass droplet evaporation becomes 7.6578% (Table 4). As one can easily see the rate of mass evaporation is higher than in both Case 16 (+1.1335%) and Case 17 (+0.5752%) depending on the droplet shrinkage increased by temperature.

Case 19 (T_a = 315 K)

The present case study relates to an air temperature of 315 K and its effect on droplet evaporation. Table 1 displays the thermophysical conditions of water and air. In this case the rate of evaporation in mass at t* = 1 is equal to 7.9084% (Table 3). Compared to the previous cases (Case 16, Case 17, Case 18) there is here an increased evaporation rate (+1.7510% with respect to Case 16, +1.1916% with respect to Case 17, +0.6069% with respect to Case 18), confirming what is qualitatively a reasonable trend: a raised air temperature value enhances aerial evaporation, keeping constant all the other parameters. Again, checking the process at a dimensionless travel distance L* = 1, reached after a time t^*_{Lmax} = 1.0476 (Table 4), droplet evaporation becomes equal to 8.2470% (Table 4). As one can easily see, this figure confirms the trend highlighted in the previous three cases: Case 16 (+1.7227%), Case 17 (+1.1644%), and Case 18 (+0.5892%) which, again, may be attributed to increased droplet shrinkage due to air temperature.
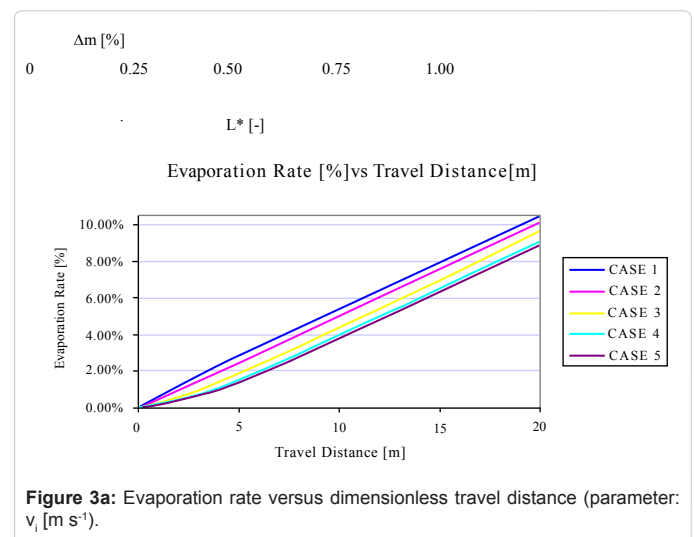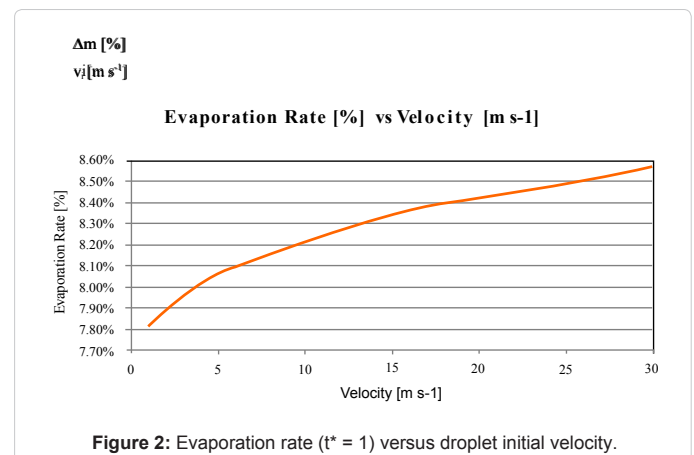
Case 20 (T_a = 320 K)

See Case 5 (duplicated case: the combination of the analysis parameters considered, leads case 20 to be coincident with case 5).

Discussion

The previous section showcased the main results that were arrived at numerically, together with a few preliminary comments that are here to be expanded for each analysis parameter. The influence of droplet initial velocity on evaporation may be inferred by comparing the results obtained in cases from 1 to 5 (Table 3). In general it may be deduced that the lower the initial velocity, the lower the evaporated mass. In detail, the evaporation rate percentage shifts from 7.8116% in Case 1 to 8.5755% in Case 5. The variation of the evaporation rate percentage against velocity shows a logarithmic trend displayed in Figure 2. Under a physical point of view such result is interpreted in the light of air friction effect both on the dynamics of vapour film surrounding the droplet and directly on evaporation (Lorenzini, 2004). Velocity enhances both convection and friction force but the latter depends on velocity raised at the second power and this makes its effect on droplet evaporation significantly more remarkable, especially for a so limited time interval as that here investigated. These comments, however, hold true just if time-dependence is analysed while if space-dependence is considered the situation changes significantly, as Figures 3a and 3b demonstrate. The following analysis is not negligible given that the present investigation has to do with a particular application, i.e. sprinkler irrigation, which is mainly interested in the spatial distribution of water for agricultural purposes. Figure 3a shows how, completing the same path, a slower droplet evaporates more than a faster one, because of a higher time of flight which acts upon water temperature

and friction. This also highlights the overlap between the effects of temperature and air friction, especially evident for faster droplets: in the first part of the flight the elevate contribution of the friction force (enhancing evaporation) does not balance the lower convective heat flux entering the droplet due to the quicker covering of the same path length. This effect becomes less significant for slower droplets, showing a linear trend, as Figure 3a displays. So, keeping the other parameters fixed, faster droplets tend to evaporate less than slower ones and consequently less water is wasted. On the contrary, Figure 3b shows that faster droplet evaporates more (especially in the first moments of flight) than slower droplet, because if the focus is on time than the friction force effect becomes predominant on ruling evaporation. From these comments it may be evicted that the phenomenon under exam is due to a dynamic and to a convective affection. The effect of droplet initial diameter on the evaporation rate may be deduced checking the cases from 6 to 10 (Table 3). In general: the bigger the diameter, the lower the evaporation mass. Evaporation rate reduction according to droplet diameter increase is remarkable, with exponential trend and results from 8.5755% (Case 6) for a 1 mm droplet diameter, to 2.1841% in the case of a 0.003 m droplet diameter (Case 10) (Figure 4). This result may be attributed to the higher thermal inertia which characterises bigger droplets, which is also bond to a less favourable surface-volume ratio (decreasing when the diameter augments). Such result may be displayed in function of the path covered (Figure 5a)

Figure 2: Evaporation rate (t* = 1) versus droplet initial velocity.

Figure 3a: Evaporation rate versus dimensionless travel distance (parameter: v_i [m s^{-1}]).

or of the simulation time (Figure 5b) which both confirm the same trend and consequent analysis. The effect of the diffusion coefficient of vapour in air on aerial water droplet evaporation was faced from Case 11 to Case 15 (Table 3). It evidently appears that, augmenting D_{va} [m^2 s^{-1}], droplet evaporation raises, as the contribution of the diffusion term is enhanced, letting evaporation rate to shift from 7.4287% (Case 11, $D_{va} = 0.2 \times 10^{-4}$ m^2 s^{-1}), to 8.5755% (Case 15, $D_{va} = 0.3 \times 10^{-4}$ m^2 s^{-1}). The trend (Figure 6) proves to be linear, in accordance to Fick's law of diffusion, keeping the coefficient constant with temperature, given the low liquid-gas interface vapour concentration gradients, typical of the phenomenon here considered. Further parametric considerations may be performed checking carefully the spatial and temporal phenomenological effects of D_{va} [m^2 s^{-1}], in Figure 7a and 7b respectively, both confirming the general trend of Figure 6. Figure 7a shows how mass evaporation raises with D_{va} [m^2 s^{-1}] for a same L* [-] value: such trend may be interpreted in relation to the necessity of keeping a constant water vapour film at the air-droplet interface by drawing it from the droplet liquid water. The curves in Figure 7a are also very close from one another, especially at the beginning of the path, i.e. for small values of L* [-]: for bigger values of L* [-] the trends tend to become more separated, as a consequence of the cumulative effects of a higher diffusion coefficient. The temporal variations displayed
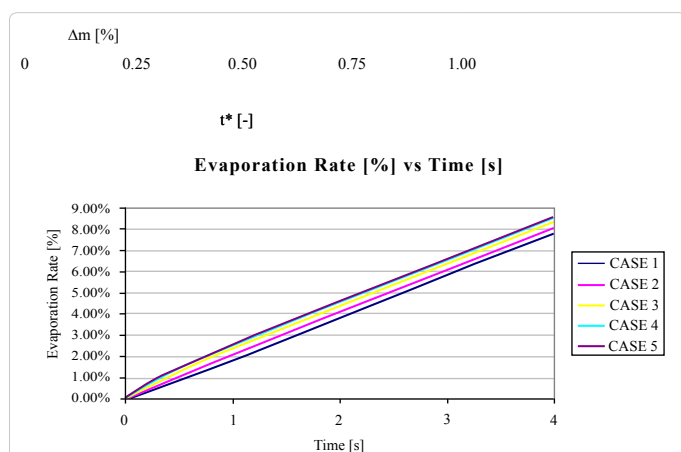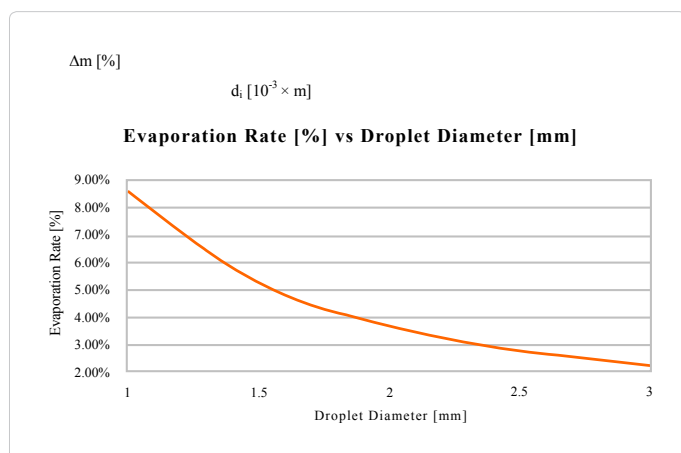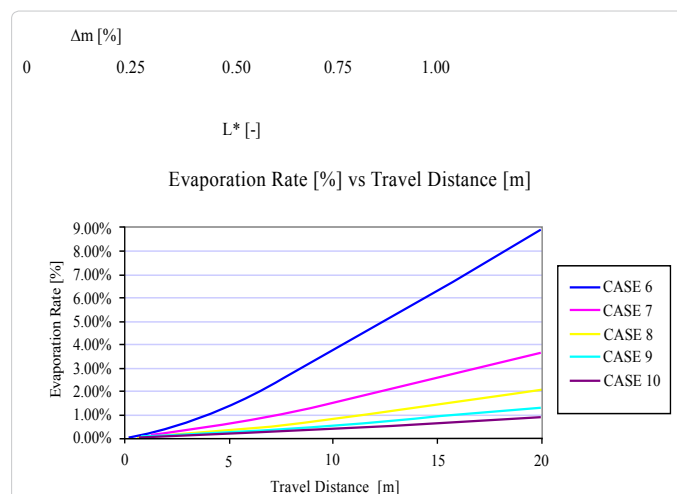

Figure 5a: Evaporation rate versus dimensionless travel distance (parameter: d_i [m]).

Figure 3b: Evaporation rate versus dimensionless simulation time (parameter: v_i [m s^{-1}]).
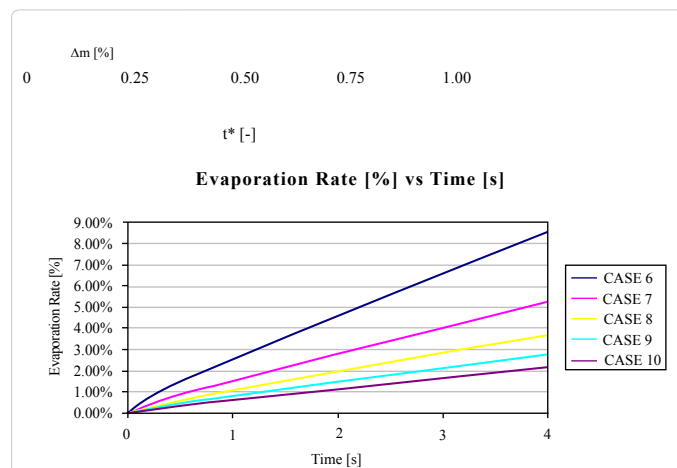

Figure 5b: Evaporation rate versus dimensionless simulation time (parameter: d_i [m]).

in Figure 7b prove similar, confirming the previously made analysis. The last parameter tested (in cases from 16 to 20) was air temperature (Table 3). When keeping all the other analysis parameters constant, droplet evaporation is promoted by air-water temperature gradient, which influences the convective contribution. In fact, varying T_a from 300 K to 320 K, evaporation augments from 6.1574% to 8.5755%, respectively. The evaporation vs. air temperature relation proves to be nearly linear (see Figure 8), which is to be attributed to the linear dependence between the temperature and the convective term in an evaporation process, in addition to the linear effect that temperature has on the entire thermal flux. As a matter of fact, as it may be deduced considering the cases study from 1 to 5, convection is a phenomenon which depends upon temperature and velocity, once the geometrical and physical features of the problem are set. The same general effect is confirmed when facing a spatial (Figure 9a) and temporal (Figure 9b) study of the parameter which is currently under examination. In particular: Figure 9a shows droplet mass evaporation rate versus the dimensionless path covered. It is confirmed a directly proportional relation between the two variables while the curves, initially very

Figure 4: Evaporation rate (t* = 1) versus droplet initial diameter.

close from one another, tend to open when getting closer to $L^* = 1$ as a consequence of the ongoing cumulative convective effect. If time dependence is investigated (Figure 9b), the general trend is the same just described even if the first moments of the path prove to be more intensely affected (with respect to the space-dependent trend of Figure 9a) by the water transient heating due to the air temperature as affecting the diffusion laws.

Conclusions

Aerial droplet evaporation is a phenomenon that applies in several technical fields related to civil, mechanical and agricultural engineering (automotive, refrigeration and conditioning, fire safety, irrigation, water saving, etc.). This study is specifically referring to irrigation and water saving, even though its results would be suitable, at least as a first step, for many other applications among those just quoted, provided that pressures and temperatures analogous to those here tested were involved. A numerical approach was employed, based on Computational Fluid Dynamics (CFD) software called STAR-CCM+ version 5.04.012: such code adopts the control volume method. The system investigated is a single spherical droplet travelling within air and evaporating during its aerial path between the nozzle and the
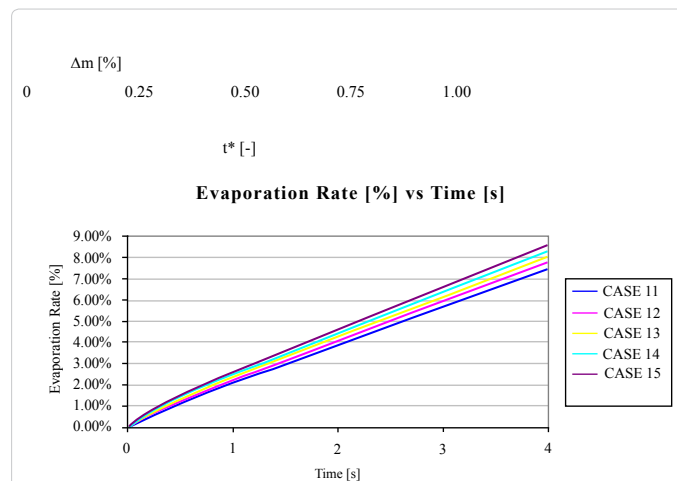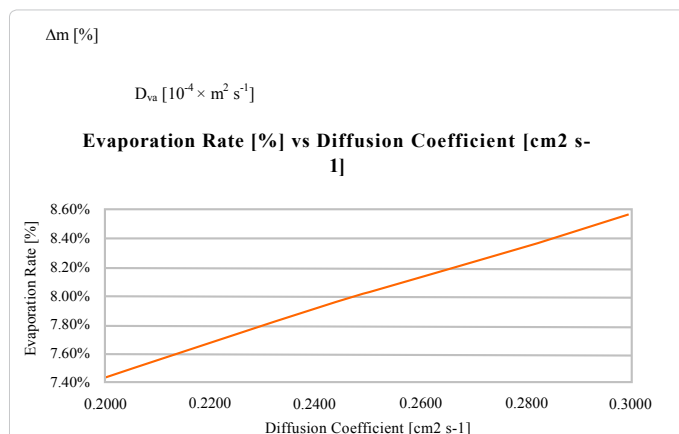

Figure 6: Evaporation rate ($t^* = 1$) versus diffusion coefficient of vapour in air.

Figure 7a: Evaporation rate versus dimensionless travel distance (parameter: D_{va} [m² s⁻¹]).

Figure 7b: Evaporation rate versus dimensionless simulation time (parameter: D_{va} [m² s⁻¹]).
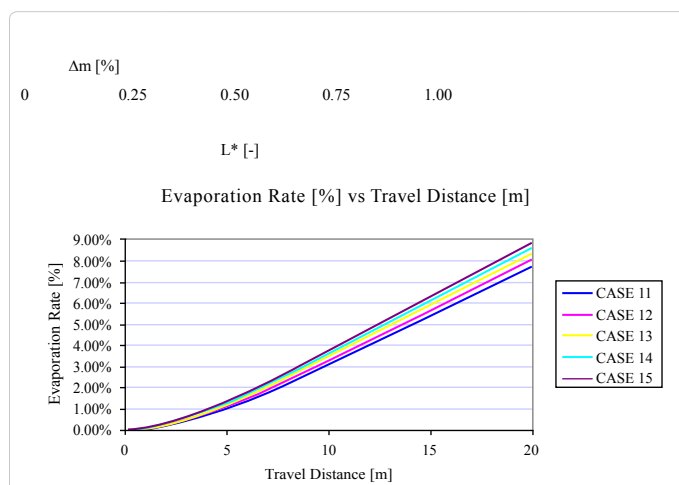

Figure 8: Evaporation rate ($t^* = 1$) versus air temperature.

ground. The analysis parameters were: droplet initial velocity; droplet initial diameter; air temperature; and diffusion coefficient of vapour in air. Air relative humidity was not a parameter here because the code proved not acceptably reliable in managing such kind of water-air interface: such limitation, anyway, does not affect the generality of the present study because of the "classical" parametric approach adopted, one variable being entirely independent on the others. Twenty cases study, five for each analysis parameter, were faced.

The results obtained show that, at the conditions tested, the parameter which affects droplet evaporation more significantly is droplet initial diameter which, varying from 0.001 to 0.003 m (a range typical in sprinkler irrigation practice), determines a droplet mass evaporation decrement of 6.3914%, considering time dependence, and 7.9331% considering space dependence: this highlights the role played in the process by the dynamic components (air friction) and by the droplet thermal inertia. Air temperature (which initially may have been suspected as the most affecting parameter) also proves significant, with a 2.4181% (time dependence considered) and 2.3253% (space dependence considered) augmentation when passing from 300 to 320 K. Droplet initial velocity (varying from 1 to 30 m s⁻¹) and diffusion coefficient of vapour in air (varying from 0.2 × 10⁻⁴ to 0.3 × 10⁻⁴ m² s⁻¹) are instead interested by an evaporation variation within the
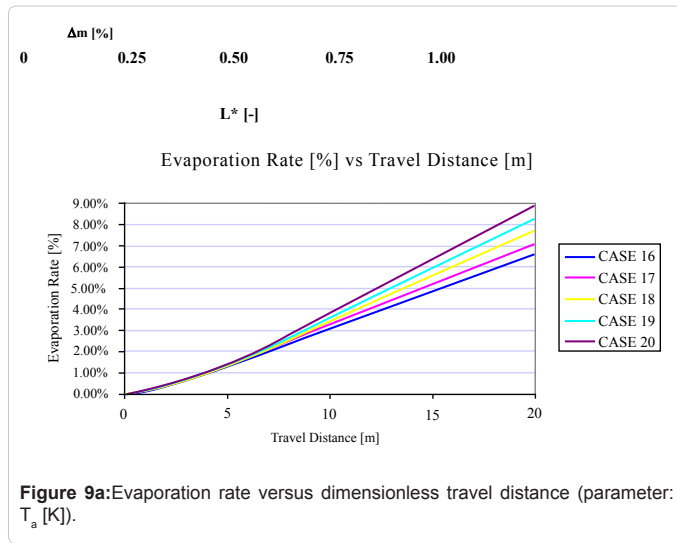
Figure 9a: Evaporation rate versus dimensionless travel distance (parameter: T_a [K]).
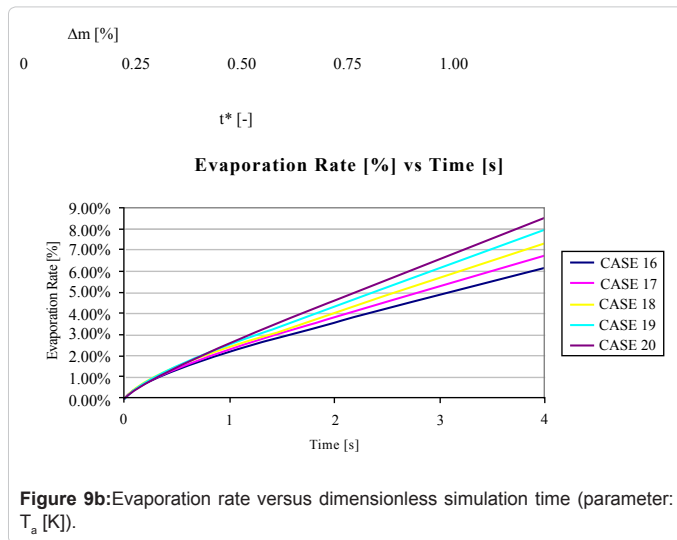

Figure 9b: Evaporation rate versus dimensionless simulation time (parameter: T_a [K]).

range investigated of 0.7639% (time dependence considered; 1.5920% when space dependence considered) and 1.1468% (time dependence considered; 1.1515% when space dependence considered), which are still significant data, anyway. Like in the case of air temperature, probably an increase of 50% in D_{va} [m^2 s^{-1}] would have suggested a much higher effect on droplet evaporation than that actually computed but the result correctly show that the droplet evaporation is a very complicate fluid dynamic process which cannot be reduced to a simply diffusive matter. Finally, for what relates to water saving in irrigation practice, one can conclude that, apart from a low air temperature and high diffusion coefficient of vapour in air condition (which, on the one hand, may have been somehow predictable but, on the other, serve to practically prove and validate the reliability of the model created and of the approach adopted) the conditions that help save water are: big droplet initial diameter and low droplet initial velocity, if the aim is that water reaches a specific location and watering covers a certain field, this (and not time) being generally the main goal which in-field irrigation wishes to achieve. Both these latter parameters, the influence of which was not predictable a priori of the present investigation, may be controlled and conditioned acting on the sprinkler operating conditions, and this makes of a numerical study a highly applicable

source to many practical issues.

Nomenclature

Symbols	Name	Unit
A:	droplet radius (Kinzer and Gunn, 1951; see Introduction)	m
A	coefficient = 11.949, (eq. 2)	-
A_p	droplet cross sectional area (eq.3)	m^2
B	coefficient = 3978.205, (eq. 2)	-
C	coefficient = -39.801, (eq. 2)	-
C_d	friction factor (eq.3)	-
CFD	Computational Fluid Dynamics	-
d_i	droplet initial diameter	m
d_p	droplet diameter, (eq.6)	m
D_{va}	diffusion coefficient of vapour in air	m^2 s^{-1}
D^	droplet diameter variation with time (Goering, 1972; see Introduction)	m s^{-1}
F_d	friction force, (eq.3)	N
G	vapour-density gradient at the droplet surface (Kinzer and Gunn, 1951; see Introduction)	kg m^{-4}
K^	ratio between D_{va} and d_p (Goering, 1972; see Introduction)	m s^{-1}
L	travel distance (eq.10)	m
L_{max}	target location (eq.10)	m
L*	dimensionless travel distance (eq.10)	-
m^	droplet mass evaporated with time (Kinzer and Gunn, 1951; see Introduction)	kg s^{-1}
m_0	droplet initial mass, (eq. 8)	kg
m_1	droplet final mass, (eq.8)	kg
M^	ratio between molecular weights of vapour and air (Goering, 1972; see Introduction)	-
Nu_p	Nusselt number (droplet), (eq. 5)	-
Nu*	specially defined Nusselt number for mass transfer (Goering, 1972; see Introduction)	-
p_{atm}	atmospheric pressure, (eq.2)	Pa
p_{sat}	saturation pressure, (eq.2)	Pa
P	difference between saturation pressure at wet bulb air temperature and vapour pressure at dry bulb temperature / partial pressure of air (Goering, 1972; see Introduction)	-
Pr_a	Prandtl number (air), (eq.5)	-
R	ratio between air and droplet density (Goering, 1972; see Introduction)	-

Re_p	Reynolds number (droplet), (eq.6)	-
Sc	Schmidt number (eq.7)	-
Sh	Sherwood number (eq.7)	-
T	time, (eq.9)	s
t^*	dimensionless time, (eq.9)	-
t_{Lmax}	simulation time after a path $L = L_{max}$, (eq. 11)	s
t^*_{Lmax}	dimensionless simulation time after a path $L = L_{max}$, (eq. 11)	-
t_{max}	maximum simulation time, (eq.9)	s
v_i	droplet initial velocity	m s^{-1}
v_p	velocity (droplet), (eq.3)	m s^{-1}
T_0	reference temperature (273.15 K), (eq.1)	K
T_a	air temperature, (eq. 1)	K
T_w	water temperature	K
Greek Symbols	**Name**	**Unit**
Δm	droplet mass evaporation rate, (eq.8)	%
μ_0	air viscosity at 273.15 K, (eq.1)	Pa s
μ_a	air viscosity (eq.1)	Pa s
ρ_a	air density (eq.3)	kg m^{-3}

References

1. Lefebvre AH (1989) Atomization and Sprays. Taylor & Francis: London.

2. Sirignano WA (1999) Fluid Dynamics and Transport of Droplet and Sprays. Cambridge University Press: Cambridge.

3. Lorenzini G (2002) Air temperature effect on spray evaporation in sprinkler irrigation. Irrigation and Drainage 51: 301-309.

4. Lorenzini G (2004) Simplified modelling of sprinkler droplet dynamics. Biosystems Engineering 87: 1-11.

5. Park TW, Aggarwal SK, Katta VR (1996) A numerical study of droplet-vortex interactions in an evaporating spray. Int J Heat Mass Transf 39: 2205-2219.

6. Abramzon B, Sirignano W (1989) Droplet vaporization model for spray combustion calculations. Int J Heat Mass Transf 32: 1605–1618.

7. Bertoli C, Migliaccio na M (1999) A finite conductivity model for diesel spray evaporation computations. International Journal of Heat and Fluid Flow 20: 552–56.

8. Gogos G, Soh S, Pope DN (2003) Effects of gravity and ambient pressure on liquid fuel droplet evaporation. Int J Heat Mass Transf 46: 283–296.

9. Sazhin SS, Krutitskii PA, Abdelghaffar WA, Sazhina EM, Mikhalovsky SV, et al. (2004) Transient heating of diesel fuel droplets. Int J Heat Mass Transf 47: 3327-3340.

10. Birouk M, Gokalp I (2006) Current status of droplet evaporation in turbulent flows. Progress in Energy and Combustion Science 32: 408-423.

11. Chen YC, Staerner SH, Masri AR (2006) A detailed experimental investigation of well-defined, turbulent evaporating spray jets of acetone. International Journal of Multiphase Flow 32: 389-412.

12. Qureshi M, Zhu C (2006) Crossflow evaporating sprays in gas–solid flows: Effect of aspect ratio of rectangular nozzle. Powder Technology 166: 60-71.

13. Sazhin SS (2006) Advanced models of fuel droplet heating and evaporation. Progress in Energy and Combustion Science 32: 162-214.

14. Sazhin SS, Kristyadi T, Abdelghaffar WA, Heikal MR (2006) Models for fuel droplet heating and evaporation: Comparative analysis. Fuel 85:1613-1630.

15. Shusser M (2007) The influence of thermal expansion flow on droplet evaporation. Heat Transfer 2: 443-449.

16. Belarbi R, Ghiaus C, Allard F (2006) Modeling of water spray evaporation: Application to passive cooling of buildings. Solar Energy 80: 1540-1552.

17. Barrow H, Pope CW (2007) Droplet evaporation with reference to the effectiveness of water-mist cooling. Applied Energy 84: 404-412.

18. Qureshi M, Zhu C (2006) Gas entrainment in an evaporating spray jet. Int J Heat Mass Transf 49: 3417-3428.

19. Chen YC, Peters N, Schneemann GA, Wruck N, Renz U, et al. (1996) The detailed flame structure of highly stretched turbulent premixed methane-air flames. Combustion and Flame 107: 223-244.

20. Rouault M, Mestayer PG, Schiestel R (1991) A Model of Evaporating Spray Droplet Dispersion. J Geophys Res 96: 7181-7200.

21. Nurnberger FV, Merva GE, Harrington JB Jr (1976) Microenviromental modification by small water droplet evaporation. Journal of Applied Meteorology 15: 858-867.

22. Edling RJ (1985) Kinetic energy, evaporation and wind drift of droplets from low pressure irrigation nozzle. Transaction of the ASABE 28: 1543-1550.

23. Thompson AL, Gilley JR, Norman JM (1993) A sprinkler water droplet evaporation and plant canopy model: II. Model application. Transaction of the ASABE 36: 743-750.

24. Lorenzini G, De Wrachien D (2003) Phenomenological analysis of sprinkling spray evaporation: the air friction effect. Rivista di ingegneria Agraria 49-54.

25. Playan E, Garrido S, Faci JM, Galan A (2004) Characterizing pivot sprinklers using an experimental irrigation machine. Agricultural Water Management 70: 177-193.

26. Lorenzini G, De Wrachien D (2004) Theoretical and Experimental analysis of spray flow and evaporation in sprinkler irrigation. Irrigation and Drainage Systems 918: 155-166.

27. Lorenzini G (2006) Water droplet dynamics and evaporation in an irrigation spray. Transaction of the ASABE 94: 545-549.

28. De Wrachien D, Lorenzini G (2006) Modeling jet flow and losses in sprinkler irrigation: overwiew and perspective of a new approach. Biosystems Engineering 94: 297-309.

29. Kinzer GD, Gunn R (1951) The evaporation, temperature and thermal relaxation-time of freely falling waterdrops. Journal of Meteorology 8: 71-83.

30. RanzWE, Marshall WR (1952a) Evaporation from drops Part I. Chem Eng Progr 48: 141-146.

31. RanzWE, Marshall WR (1952b) Evaporation from drops Part II. Chem Eng Progr 48: 173-180.

32. Dzumbova L, Schwarz J, Smolik J (1999) Evaporation of water droplet in the humid atmosphere. J Aerosol Sci 30: S337–S338.

33. McLean RK, Sri Ranjan R, Klassen G (2000) Spray evaporation losses from sprinkler irrigation systems. Canadian Agricultural Engineering 42: 1.1-1.15.

34. Carrion P, Montero J, Tarjuelo JM (2001) Applying simulation on sprinkling irrigatuion systems design: SIRIAS model. Revista Internacional de Métodos Numérico para Calculo y Diseno en Ingenieria 17: 347–362.

35. Qu X, Davis EJ, Swanson BD (2001) Non-isothermal droplet evaporation and condensation in the near-continuum regime. J Aerosol Sci 32: 1315–1339.

36. Moyle AM, Smidansky PM, Lamb D (2006) Laboratory studies of water droplet evaporation kinetics. In: Proceeding of 12th Conference on Cloud Physics, and Proceeding of 12th Conference on Atmospheric Radiation. American Meteorological Society.

37. Yan HJ, Bai G, He, JQ, Li YJ (2010) Model of droplet dynamics and evaporation for sprinkler irrigation. Biosystems Engineering 106: 440-447.

38. Goering CE, Bode LE, Gebhard MR (1972) Mathematical modeling of spray

droplet deceleration and evaporation. Transactions of the ASAE 15: 220-225.

39. Sirignano WA (1993) Fluid dynamics of sprays—1992 Freeman scholar lecture. Transaction of the ASME- J Fluids Eng 115: 345-378.

40. Kulmala M, Vesala T, Schwarz J, Smolik J (1995) Mass transfer from a drop-II. Theoretical analysis of temperature dependent mass flux correlation. Int J Heat Mass Transf 38: 1705-1708.

41. Gouesbet G, Berlemont A (1999) Eulerian and Lagrangian approaches for predicting the behaviour of discrete particles in turbulent flows. Progress in Energy and Combustion Science 25: 133-159.

42. Dombrovsky LA, Sazhin SS (2003) A simplified non-isothermal model for droplet heating and evaporation. International Communications in Heat and Mass Transfer 30: 787-796.

43. Kolaitis DI, Katsourinis DI, Founti MA (2009) Droplet evaporation assisted by "stabilized cool flames": scrutinizing alternative CFD modelling approaches. Seventh International Conference on CFD in the Minerals and Process Industries (CSIRO, Melbourne, Australia, 9-11 December).

44. Edson JB, Anquetin S, Mestayer PG, Sini, JF (1996) Spray droplet modelling 2. An interactive Eulerian-Lagrangian model of evaporating spray droplets. J Geophys Res 101: 1279-1293.

45. Burger M, Rottenkolber G, Schmehl R, Giebert D, Schaefer O, et al. (2002) A Combined Eulerian and Lagrangian Method for Prediction of Evaporating Sprays. J Eng Gas Turbines and Power 124: 481-488.

46. Salman H, Soteriou M (2004) Lagrangian simulation of evaporating droplet sprays. Physics of Fluids 16: 4601–4622.

47. Beck JP, Watkins AP (2003) The droplet number moments approach to spray modelling: The development of heat and mass transfer sub-models. International Journal of Heat and Fluid Flow 24: 242-259.

48. Okamura S, Nakanishi K (1969) Theoretical study on sprinkler sprays (part four) geometric pattern form of single sprayer under wind conditions. Transactions of the Japanese Society of Irrigation Drainage and Reclamation Engineering 29: 35-43.

49. de Lima JLMP, Torfs PJJF, Singh VP (2002) A mathematical model for evaluating the effect of wind on downward-spraying rainfall simulators. Catena 46 : 221-241.

50. Miliauskas G, Sabanas V (2006) Interaction of transfer processes during unsteady evaporation of water droplets. Int J Heat Mass Transf 49: 1790-1803.

51. Sutherland W (1893) The viscosity of gases and molecular force. Philosophical Magazine 5 36: 507-531.

52. Star-CCM+, version 5.04.012, (2010) Users' Guide.

53. Reid RC, Prausnitz JM, Poling BE (1988) The Properties of Gases and Fluids. (2ndedn), Mc-Graw Hill: New York.

54. Schiller L, Naumann A (1933) Ueber die grundlegenden Berechnungen bei der Schwerkraftaufbereitung. VDI Zeits 77: 318-320.

55. Bird RB, Stewart WE, Lightfoot EN (2006) Transport Phenomena. (4thedn), Wiley and Sons: New York.

56. Carmichhael LT, Sage BH, Lacey WN, (1955) Diffusion coefficients in hydrocarbon systems: n-Hexane in the gas phase of the methane—, ethane—, and propane—n-hexane systems. AIChE 1: 385-390.

57. Wilke CR, Lee CY (1955) Estimation of Diffusion Coefficients for Gases and Vapors. Ind Eng Chem 47: 1253-1257.

58. Fuller EN, Giddings JC (1965) A comparison of methods for predicting gaseous diffusion coefficients. Journal of Gas Chromatography 3: 222-227.

59. Fuller EN, Schettler PD, Giddings J C (1966) A new method for prediction coefficients of binary gas-phase diffusion Ind Eng Chem 58: 18-27.

60. Fuller EN, Ensley K, Giddings J C (1969) Diffusion of halogenated hydrocarbons in helium. The effect of structure on collision cross sections. J Phys Chem 73: 3679-3685.

61. Green DW, Perry RH (2008) Perry's Chemical Engineer's Handbook. (8thedn), McGraw-Hill: New York.

62. Keller J, Bliesner RD (1990).Sprinkler and Trickle Irrigation. Van Nostrand Reinhold: USA.

63. Salvador R, Bautista-Capetillo C, Burguete J, Zapata N, Serreta A, et al. (2009) A photographic method for drop characterization in agricultural sprinklers. Irrigation Science 27: 307-317.

64. Babinsky E, Sojka PE (2002) Modeling droplet size distribution. Progress in Energy and Combustion Science 28: 303-329.

65. DeBoer DW, Monnens MJ, Kincaid DC (2001) Measurement of sprinkler droplet size. Appl Eng Agric 17: 11-15.

66. DeBoer DW (2002) Drop and Energy Characteristics of a Rotating Spray-Plate Sprinkler. J Irrig Drain Eng 128: 137-146.